NANO LETTERS

ACS AUTHORCHOICE

pubs.acs.org/NanoLett

Letter

Projection Microstereolithographic Microbial Bioprinting for Engineered Biofilms

Karen Dubbin, Ziye Dong, Dan M. Park, Javier Alvarado, Jimmy Su, Elisa Wasson, Claire Robertson, Julie Jackson, Arpita Bose, Monica L. Moya, Yongqin Jiao, and William F. Hynes*

Cite This: *Nano Lett.* 2021, 21, 1352−1359

Read Online

ACCESS | Metrics & More | Article Recommendations | Supporting Information

ABSTRACT: Microbes are critical drivers of all ecosystems and many biogeochemical processes, yet little is known about how the three-dimensional (3D) organization of these dynamic organisms contributes to their overall function. To probe how biofilm structure affects microbial activity, we developed a technique for patterning microbes in 3D geometries using projection stereolithography to bioprint microbes within hydrogel architectures. Bacteria were printed and monitored for biomass accumulation, demonstrating postprint viability of cells using this technique. We verified our ability to integrate biological and geometric complexity by fabricating a printed biofilm with two *E. coli* strains expressing different fluorescence. Finally, we examined the target application of microbial absorption of metal ions to investigate geometric effects on both the metal sequestration efficiency and the uranium sensing capability of patterned engineered *Caulobacter crescentus* strains. This work represents the first demonstration of the stereolithographic printing of microbials and presents opportunities for future work of engineered biofilms and other complex 3D structured cultures.

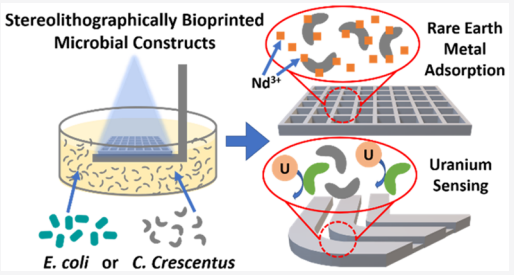

KEYWORDS: *Bioprinting, Additive Manufacturing, Microbial Printing, Biofilm, Biosensor, Bioremediation, Stereolithography, Bacteria*

Biofilms are complex communities of one or more microbial species ensconced in extracellular polymeric substances (EPS) consisting of both polymer and protein components.[1] Bacterial biofilms have long been of interest to scientists and engineers,[2] both for their unique communal structure and the potential to harness these microbial films for human-impact applications such as generation of organic products and environmental remediation.[3−5] Compared to current inorganic methods for these types of applications, biofilm alternatives may offer a lower cost and minimize the use of harsh chemicals. Microbiologists have investigated artificial biofilms to better control events such as cell−cell communication,[6] but these have generally lacked direct control over the resulting film geometry, which limits interrogation of these events to either simplified or well-mixed conditions.

Microbes grown in biofilms show unique behaviors due to complex interactions between constituent film members and their environment.[7] For instance, microbes within a biofilm can engage in gene transfer between member cells and demonstrate increased antimicrobial resistance.[8,9] Three-dimensional (3D) organization becomes especially interesting given that spatial distribution of microbes can influence community stability[6] and biodiversity in microbial consortia.[10] While laboratory cultivation of biofilms is a common practice, existing culture methods lack the ability to engineer the density and structural complexity of the resulting bacterial biofilms.[11] In natural biofilm architecture, different microbial species grow in colonies with submillimeter spacing.[12] This differs from the homogeneous culture of microbial communities common to laboratory culture, where different species may be required to compete for nutrients in a "survival of the fittest" scenario.[6] Given the unique microbial functions enabled by biofilm growth, there is great interest in generating complex structured cultures of microbes in a controlled, reproducible manner.

Three-dimensional printing of microbes has recently become a new thrust area for biological additive manufacturing, and with it, new possibilities for culturing and manipulating microbes have begun to emerge.[13−17] Patterning biological components in 3D offers the ability to alter and augment transport of various components from ions to small molecules within a structure. As a result, the establishment of geometrically defined culture conditions permits physical entrapment of cells within high surface-area-to-volume ratio constructs enabling enhanced nutrient flux, efficient biocatalytic activity, and the opportunity to evaluate microbial growth within a defined 3D matrix. While printing of biomaterials is well documented, the focus thus far has primarily been upon tissue

Received: October 14, 2020
Revised: January 14, 2021
Published: January 28, 2021

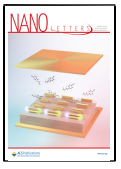

https://dx.doi.org/10.1021/acs.nanolett.0c04100
Nano Lett. 2021, 21, 1352−1359

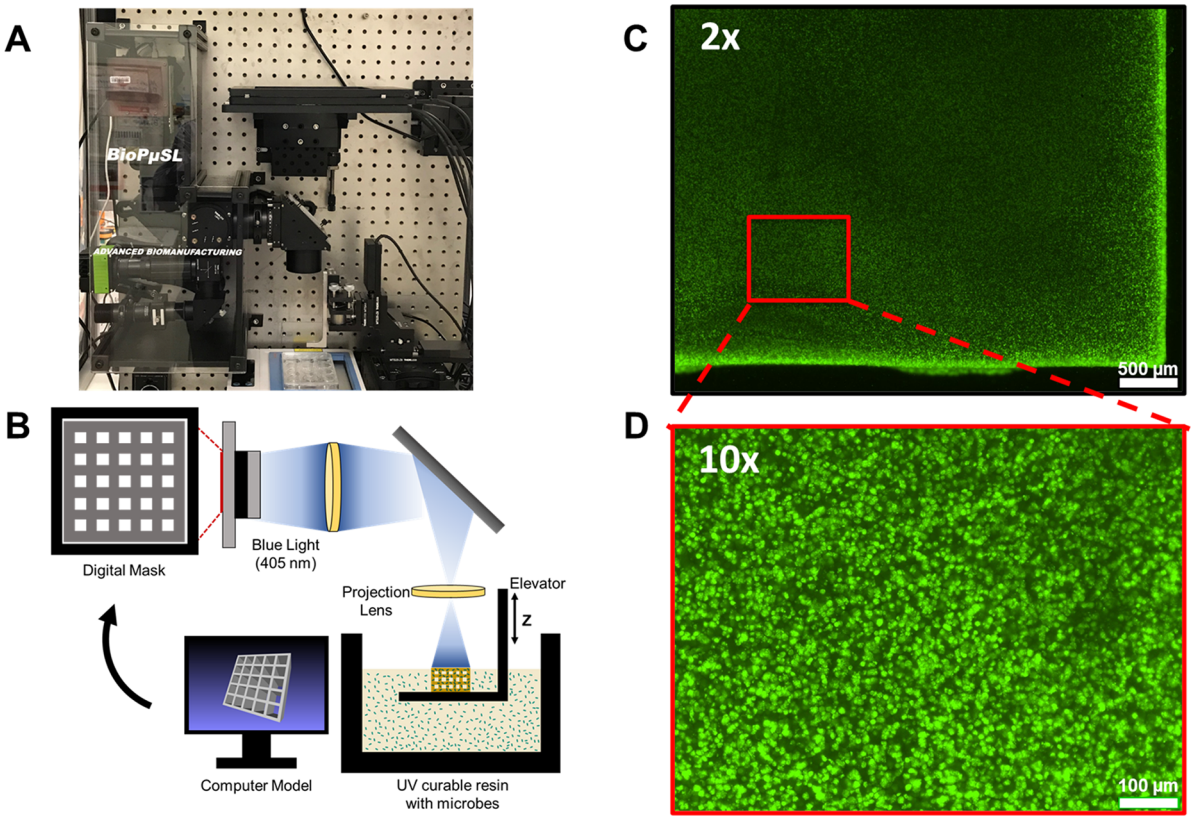

Figure 1. Demonstration of the stereolithographic apparatus for microbial (SLAM) bioprinting. Photograph of the Bio-PμSL printer used for SLAM printing (A). Schematic of the SLAM bioprinting process (B). Demonstration of the engineered biofilm using encapsulated *E. coli* expressing GFP (green) under 2× magnification (C) or 10× magnification (D).

engineering for human regenerative medicine applications.[18−22] By extending the bioprinting approach from tissue engineering to microbial culture engineering, new opportunities for exerting spatiotemporal control over the dynamic microbe environment and microbial population-level interactions can be realized.

Despite the recent surge of experimental work on microbial bioprinting, no single approach or technique is yet able to rapidly generate macroscale 3D, microbial-laden structures capable of mimicking the geometry of microbial biofilms like those found pervasively throughout nature. The most explored method of microbial bioprinting thus far has been extrusion-based methods.[13,16,23] While this approach has been beneficial to engineer 3D properties such as porosity or surface-area-to-volume ratio,[16,23] extrusion-based approaches utilizing polymer-based inks are limited to a relatively coarse resolution (>100 μm thick). In contrast, biofilms are typically between 3 and 1000 μm in depth.[24] To overcome this limitation, other printing technologies such as inkjet,[25] laser-assisted,[26,27] and contact printing methods[28,29] have been explored. While these techniques achieve better control over XY printing, achieving micrometer-scale resolution, these methods are largely restricted to two-dimensional patterning making them unsuitable for engineering biofilms. Multiphoton photolithography is the only current 3D bacterial bioprinting method with the precision required to generate biofilm-sized structures,[30] however, this approach requires user expertise and expensive, highly specialized equipment not commonly available in laboratories. Furthermore, this technique is time-consuming compared to the other fabrication methods described above, which limits its feasibility for sample generation in larger-scale experimentation or industrial use.

Here, we report a new bioprinting technique to pattern microbial constructs: stereolithographic apparatus for microbial bioprinting (SLAM Bioprinting). SLAM is capable of rapidly patterning engineered biofilms with areas of >48 mm^2, micrometer-scale X-Y resolution, and thicknesses ranging from 10 μm to >5 mm. This work expands upon previous stereolithographic (SLA) techniques which have become increasingly available in laboratory settings,[31] applying them for the first time to microbial bioprinting. Using this approach, we demonstrate viable patterning and subsequent growth of *E. coli* bacteria within 3D bioprinted, bacteria-laden biofilms. We show how altering biofilm geometry influences mass transport to govern example applications of metal ion absorption for rare earth metal recycling and uranium sensing. This enabling technology opens the door to the concepts of rationally designed, artificial biofilms possessing defined geometric characteristics. Using SLAM, spatially controlled studies of microbial behaviors and environmental responses within the context of a living engineered biofilm can be performed. These films have broad applicability including in biomanufacturing, living biosensors, bioremediation, and fundamental microbiology.

Projection microstereolithography (PμSL), a layer-by-layer additive technique that uses photopolymerizable resins, is a rapidly developing method to create complex 3D architectures.[31−33] SLAM bioprinting utilizes a custom-built biological PμSL (BioPμSL) system which uses an LED projector with a 405 nm wavelength light source to project an image onto a

https://dx.doi.org/10.1021/acs.nanolett.0c04100
Nano Lett. 2021, 21, 1352−1359

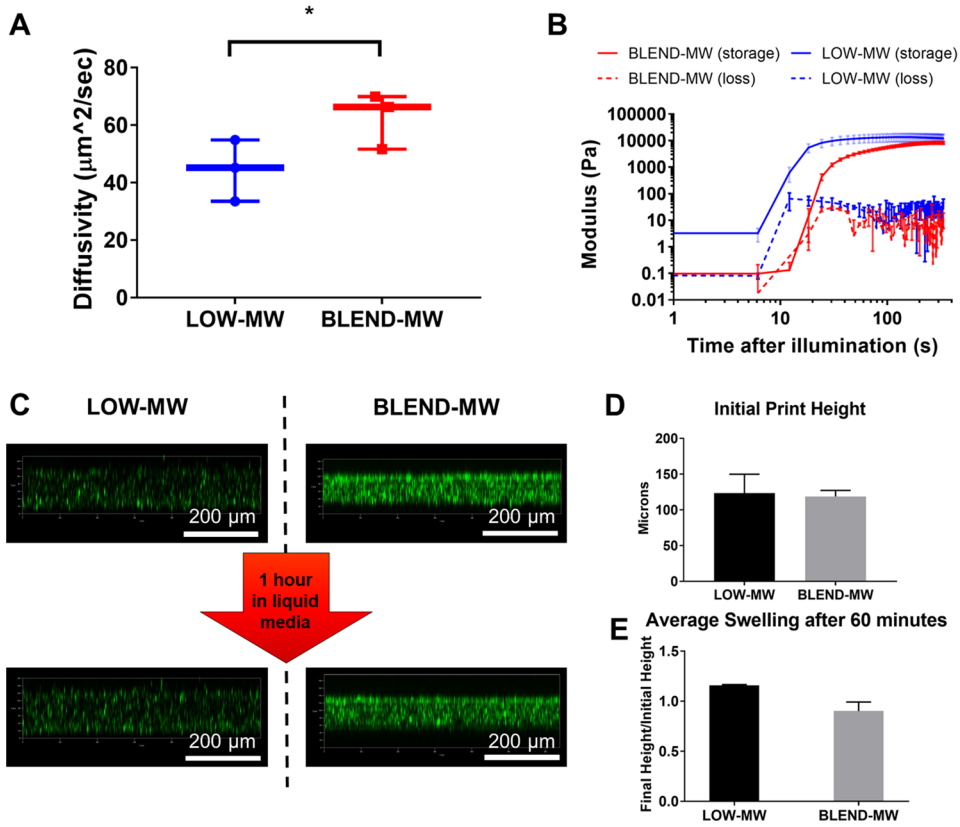

Figure 2. Resin characterization. Diffusivity of 3 kDa FITC-dextran in LOW-MW and BLEND-MW resins (A). UV rheology showing mechanical properties after exposure to 405 nm light (B). Characterization of cured resins in LB media after 60 min. Side view of confocal z-stacks of printed structures after incubation (C) along with the characterization of the initial print height (D) and the average change in height after incubation (E).

thin layer of liquid bioresin (Materials and Methods a). The projected light polymerizes the resin into a hydrogel, providing structure to the encapsulated microbes (Figure 1). Using SLAM, we have printed constructs with layer thicknesses as low as 10 μm, which is well within the range of natural microbial biofilm thicknesses. The visible violet wavelength was chosen due to its compatibility with known biocompatible photoinitiators and its low cytotoxicity compared to shorter wavelengths.[34] In this work we used a photoinitiator final concentration of 0.1% (w/v) lithium phenyl-2,4,6-trimethylbenzoylphosphinate (LAP) in phosphate buffered saline. Quinoline yellow (QY), a yellow food dye, is used as a photoabsorber at concentrations between 0.01 and 0.04% (w/v) for various formulations, as noted.

Two synthetic matrices composed of poly(ethylene glycol) diacrylate (PEGDa) were chosen as bioresins and EPS mimics given their tunability, versatility, and previous use in microbial encapsulation studies.[35,36] The polymer component consisted of either 10% (v/v) PEGDa 700 referred to as LOW-MW resin or a mixture of both the higher (5% (w/v) PEGDa 6000) and the lower molecular weight PEGDa (5% (v/v) PEGDa 700) and referred to as the BLEND-MW resin. These two formulations were chosen to provide differing material properties to probe the effect properties such as diffusion and swelling have on growth within printed structures. As cells become surrounded by EPS during biofilm formation, the mechanical properties they experience are inherently different from planktonic culture,[37] with some species able to sense this environmental shift.[38] By altering the molecular weight of the PEGDa used in the resins, the total number of acrylate groups available for cross-linking can be modified, while total polymer percentage remains constant, likely influencing both the modulus and transport properties within the cross-linked construct.

To test these properties, fluorescence recovery after photobleaching (Materials and Methods e) and UV rheology (Materials and Methods f) were used to evaluate the diffusivity and moduli of the printed resins, respectively. The LOW-MW resin produced constructs with lower diffusivity (44.5 ± 10.7 μm^2/sec) compared to the BLEND-MW resin (62.6 ± 9.7 μm^2/s). This suggests that increasing the average molecular weight of the bioresin polymers, while keeping both the initiator and the photoabsorber concentration constant, leads to greater porosity within the final hydrogel (Figure 2A,B). Given the nanoscale hydrodynamic radius of the dextran used,[39] we hypothesize that the cured resins exhibit nanometer scale pore size, consistent with previous studies of PEGDa hydrogels.[40,41] This nanoscale porosity serves to confine the encapsulated microbes, while still readily permitting diffusion of nutrients and waste. Similarly, the LOW-MW resin leads to a higher final storage modulus (12160 ± 6900 Pa) when compared to our BLEND-MW resin (8260 ± 825 Pa) (Figure 2B), consistent with previous reports on the effect of changing the polymer molecular weight on hydrogel stiffness.[41]

An *E. coli* strain that constitutively expresses the green fluorescent protein (GFP) was used to visualize the cell position within the printed construct. Microbes were incorporated into bioresins as described in Materials and Methods b. For swelling measurements, a simple cell-laden square geometry was printed, followed by confocal microscopy

https://dx.doi.org/10.1021/acs.nanolett.0c04100
Nano Lett. 2021, 21, 1352−1359

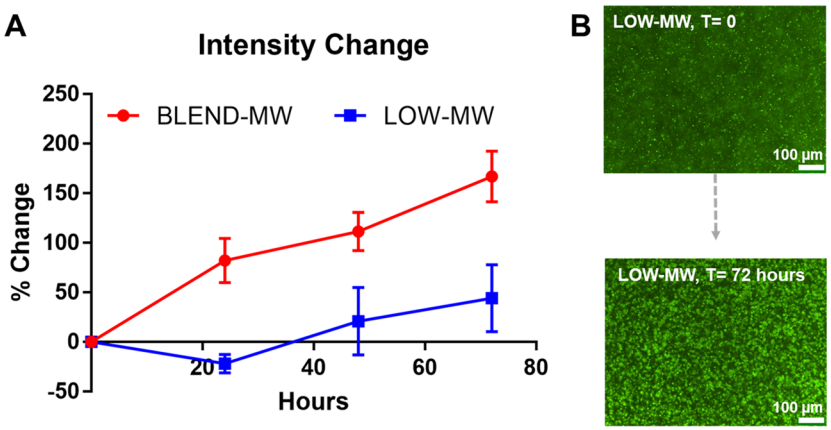

Figure 3. Viable biomass accumulation over time. Intensity change of GFP over time (A) and images of microbes in printed biofilms at 0 and 72 h (B).

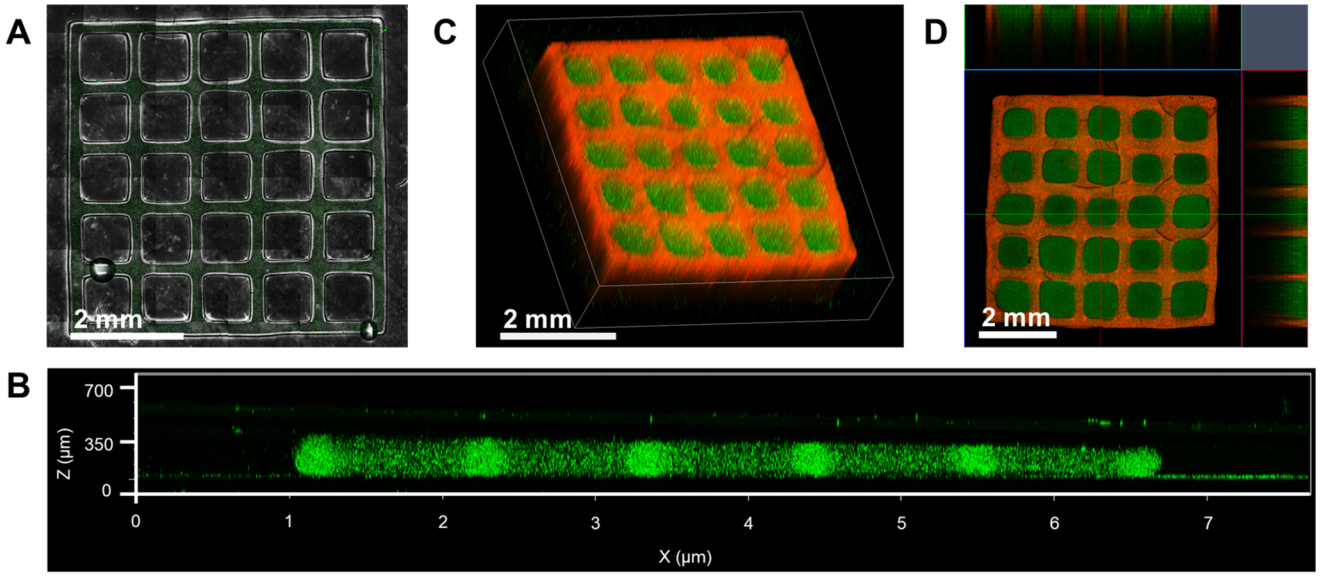

Figure 4. Demonstration of the engineering complexity in SLAM-printed biofilms. Top down (A) and side view (B) confocal z-stack images of grid geometry with encapsulated *E. coli* expressing GFP (green) showing increased print complexity, rotated view (C), and top down view with side views inset (D) confocal z-stacks of dual species print with encapsulated *E. coli* expressing either GFP (green) or mCherry (red).

to measure the initial height of the structure (Figure 1C). These structures were then incubated in Lysogeny Broth (Miller; LB) for 1 h to monitor for any subsequent swelling of printed hydrogel structures. After incubation, minimal (<10%) swelling was observed in the *Z*-direction in both resins after quantification using ImageJ software (National Institute of Health, Bethesda, MD) (Figure 2C,D,E). These results demonstrate maintenance in structural fidelity of the printed structure within the culture media over 1 h. This feature is critical to controlled biofilm studies as both the film thickness and transport properties should directly affect the growth and metabolic dynamics of the entrapped microbes.

To explore the growth of the encapsulated microbes within this 3D environment, fluorescence intensity resulting from the printed *E. coli*'s constitutive expression of GFP was used as a proxy for biomass accumulation over time.[28] *E. coli* was printed in square geometries before cultivation in LB broth at 30 °C for 3 days (Materials and Methods d). Over the culture period, increased fluorescence intensity was observed in both resins. Interestingly, the fluorescence readings in prints using LOW-MW resin showed a dip in overall fluorescence 24 h after printing, with the fluorescence recovering by 48 h in culture (Figure 3). Though initial printing may introduce a period of low cell growth in the LOW-MW resin, the return to increasing biomass suggests that any extended lag phase or toxicity experienced due to the printing process is overcome within 48 h. That the BLEND-MW resin does not exhibit such a decrease in fluorescence suggests its enhanced diffusivity plays a role in limiting the postprinting lag phase or possible toxicity.

Structures printed in the BLEND-MW resin exhibited greater biomass accumulation than those encapsulated in the LOW-MW resin, as evidenced through a larger percent intensity change (Figure 3). Microbes encapsulated in the LOW-MW resin grow as smaller, discrete colonies, while microbes in the BLEND-MW resin form larger microcolonies that overlap with one another (Figure S1), qualitatively demonstrating the effect of the bioresin composition on microbe microcolony formation. These results are consistent with the diffusivity data, suggesting both nutrients and waste metabolites are transported more rapidly within the BLEND-MW resin and are consistent with previous work on the effect of hydrogel mechanical properties on artificial biofilm gels.[41]

https://dx.doi.org/10.1021/acs.nanolett.0c04100
Nano Lett. 2021, 21, 1352−1359

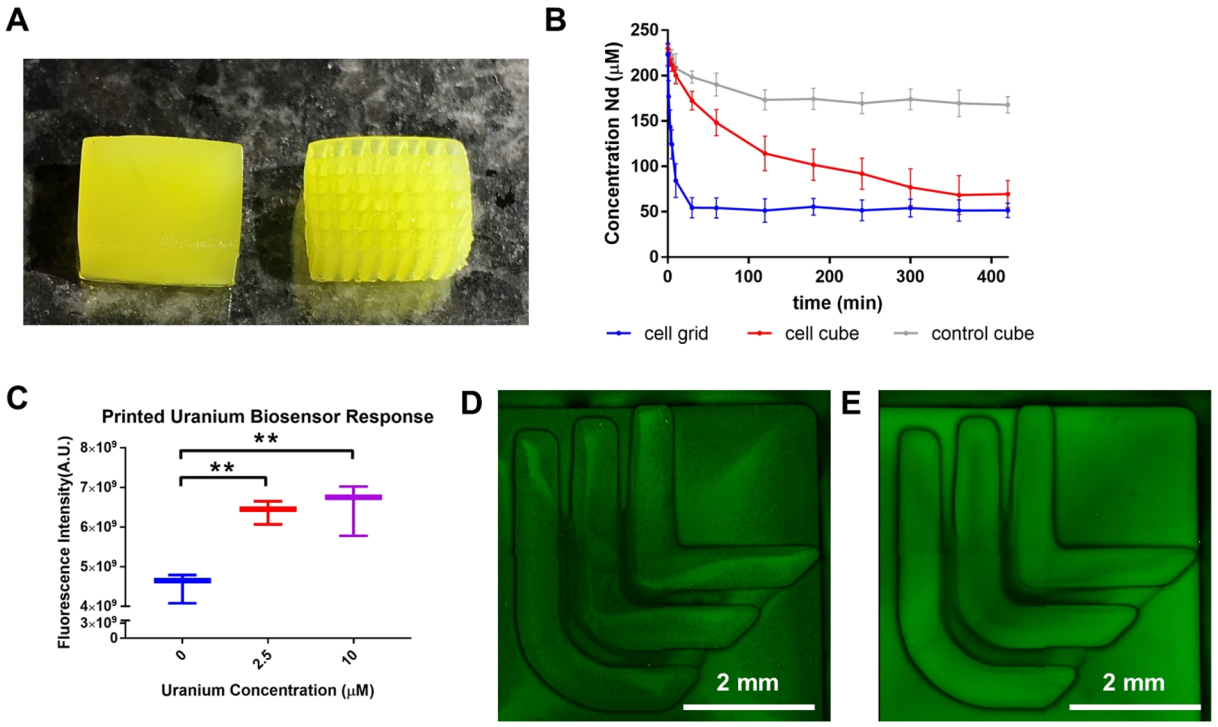

Figure 5. SLAM bioprinted biofilms can be used for functional applications including microbial adsorption and sensing. Toward absorption of rare earth elements, engineered *C. crescentus* was encapsulated in two different geometries for neodymium absorption. Macroscale image of the cell-laden, SLAM printed cube (left) and grid (right) geometries (A). Concentration of neodymium within cell-laden constructs showing increased absorption by cells within the grid geometry compared to cells encapsulated in a cube (B). Each sample was reused 3 times to create sample replicates. Toward microbial sensing, *C. crescentus* engineered for uranium sensing was encapsulated in the BLEND-MW resin and exposed to three concentrations of the uranium solution. The resulting fluorescence intensity shows an increased fluorescence for 2.5 and 10 μM uranium compared to the no uranium exposure control (C). An LLNL logo print with encapsulated *C. crescentus* either not exposed to uranium (D) or exposed to 10 mM uranium (E). ** denotes *p*-value <0.01.

Furthermore, mechanical stiffness of these materials may play a role in microbe growth. While cells encapsulated within the LOW-MW resin may experience slower nutrient transport, using a lower molecular weight PEGDa may result in a construct with greater print fidelity, as stiffer gels have been previously linked to better pattern fidelity.[42] Future work in this area includes further modulation of material properties by changing the PEGDa molecular weight or concentration, or incorporating additional polymer species is possible.

Some bacteria can sense the mechanical properties of their environment as part of their surface detection mechanisms.[37,43,44] For example, cell adhesion showed an inverse relationship with the substrate modulus for *Staphylococcus aureus*.[45] Many works exploring EPS material properties on embedded bacterial behavior are limited to a rheological investigation of full biofilms,[46,47] which obfuscates the modulus contributions from the EPS versus from the cells themselves. One work demonstrated an inverse correlation among the encapsulating gel modulus, growth rate, and cell elongation in *E. coli*.[48] While increasing agarose gel weight percent increases the modulus in these gels, a corresponding change in pore size and tortuosity makes it difficult to conclude stiffness alone was responsible for decreased growth rate. These results are consistent with our findings, which suggests an inverse relationship between biomass accumulation and gel modulus.

To demonstrate the flexibility of the SLAM technique, we increased the biofilm print complexity using a gridded geometry, increasing the surface area available within the printed biofilm (Figure S2). The 5 by 5 unit square grid features a unit cell of 800 μm voids with 200 μm thick walls and a 2.5 mm height (Figure 4A). Even when modifying the geometry, a homogeneous distribution of the encapsulated fluorescent *E. coli* was observed throughout the printed construct (Figure 4B). Geometric features, such as voids, likely affect the nutrient transport and availability within the biofilm. To explore this further, we developed a COMSOL model of the grid and square geometries showing faster diffusion of nutrients within the grid construct, due to the greatly increased surface area (Figure S3, Materials and Methods i). Using the SLAM technique, we can print biofilms at a range of thicknesses with control over transport of nutrients or soluble signaling molecules for cell behavior modulation, paving the way for the exploration of increasingly complex biofilm geometries.

Given the importance of organization in microbial communities, we next utilized SLAM bioprinting to pattern multiple strains within one biofilm. To this end, two strains of fluorescent *E. coli* were used for the construct. The first strain, constitutively expressing mcherry, was printed within a grid geometry with the print parameters described in Supporting Information h. The second resin, laden with *E. coli* which constitutively expresses GFP, was then infilled into the voids of the grid geometry followed by photopolymerization cross-linking for 30 s. In doing so, distinct microbial communities were able to be patterned with defined geometries within a designed, printed bionetwork (Figure 4). Future work using SLAM will allow for precise control over the microbial population ratios within rationally designed biofilms, enabling

https://dx.doi.org/10.1021/acs.nanolett.0c04100
Nano Lett. 2021, 21, 1352−1359

the in-depth study of species−species or strain−strain interactions in 3D that are challenging to decouple in natural biofilms.

To illustrate the importance of the geometry on the microbial construct function, we compared absorption of rare earth elements (REEs) in bioprinted constructs possessing differing geometries. REEs such as yttrium, lanthanum, and neodymium play an essential role in many technologies ranging from consumer technologies to renewable energy sources.[49,50] Due to its relevance to technological applications, the demand for REEs has continued to rapidly increase since the 1960s.[51] Recently, microbe-based REE recovery has gained increasing attention due to its low cost and environmental friendly nature compared with traditional REE extraction methods.[35] To determine if manipulating the geometry of the encapsulated microbes may offer greater control over the absorptive properties of these cells, we utilized a previously reported strain of nonviable *Caulobacter crescentus* engineered to express lanthanide binding peptides, enabling selective absorption of lanthanides over non-REEs.[35] Microbes were encapsulated in 5% (w/v) PEGDa 6 kDa and 10% (v/v) PEGDa 700, creating a BLEND-15% resin to compensate for extremely dense bacterial loading within the resin, which was then printed into both grid and cube geometries. Multiple cell-laden grid and cube geometries were printed to achieve a total volume of 500 μL (Figure 5A).

Batch adsorption experiments where conducted to demonstrate the advantage of the patterned structure generated by using SLAM. Cell-laden grids and cubes were exposed to a neodymium (Nd) solution while the depletions of Nd were tracked over time, as described in Materials and Methods j. In both geometries (Figure 5B), soluble Nd decreased during incubation with the structures, indicating Nd diffusion into gels and adsorption onto cells. Comparing the two geometries, a substantially steeper adsorption curve was obtained by the grid structure with a $T_{1/2}$ of 5 min of incubation, compared to 120 min with the cube print (Figure 5A). The same prints were reused after desorption of the Nd for subsequent measurements for a total of three technical replicates. Although approximately equal Nd adsorption capacities were achieved after 7 h, the slower kinetics of the cube structure limits its utility for REE remediation applications. These results support our initial hypothesis and demonstrate that cells printed in the grid geometry can passively adsorb REE with much more rapid absorption kinetics, relative to bulk hydrogels, both through an increased surface area-to-volume ratio and decreased diffusion distance. Additionally, the ability to reuse these printed constructs for Nd adsorption and reclamation makes them ideal for REE remediation applications.

To further highlight the utility of the SLAM technique, we next printed living, microbe-based uranium sensors. Uranium is used in many applications ranging from fuel for nuclear energy sources to radioisotopes for medical application. Despite its common use, uranium is toxic as a radioisotope and as a heavy metal; therefore, the accidental release of uranium into the environment poses a health threat to humans.[52] Despite governmental limits on the amount of uranium allowable in groundwater, these limitations can be hard to enforce given the difficulty in monitoring the environmental levels. Microorganisms engineered to rapidly sense uranium offer a cost-effective means for uranium sensing to offer *in situ* monitoring of the uranium concentration in groundwater.

For our printed uranium biosensor, we incorporated a previously developed *C. crescentus* strain containing a transcriptional fusion between the uranium-responsive promoter P_{phyt} and *gfp*.[53] This strain, in response to uranium exposure, expresses GFP, resulting in measurable fluorescence. *C. crescentus* was printed within a cubic structure and exposed to three different concentrations of uranium (Figure 5C). In response to uranium, sensors exposed to 2.5 μM and 10 μM uranium exhibited significantly higher fluorescence compared to the control prints. We then printed encapsulated the engineered *C. crescentus* strain using an .stl file depicting the LLNL logo and exposed the resulting print to 0 μM (control, Figure 5D) or 10 μM (Figure 5E) as a demonstration of the SLAM's ability to print increasingly complex structures. While there is some background fluorescence in the control print, increased fluorescence intensity can be observed after uranium exposure.

In summary, we report a novel method for 3D patterning of microbes using SLAM bioprinting to study and harness engineered biofilms in a laboratory setting. Using this technique, we were able to reproducibly print biofilm-scale constructs using bioresins with varying mechanical properties. This technique enables biofilm fabrication with live microbes, which can be maintained through at least 3 days in culture. Furthermore, we show a proof-of-concept using this technology to design microbial communities, patterning multiple microbial species within a printed film. The potential applications for this type of engineered ecosystem range from studying basic biological questions to harnessing biology for medical, biomanufacturing, energy, or environmental applications. Finally, as a demonstration of the potential for energy and environmental applications, we show the benefit of the engineered complexity within cell-laden hydrogels for absorption of rare-earth metals and uranium sensing. This concept can be further applied to a range of additional environmental remediation applications harnessing the unique capabilities of microbes in a controlled manner.

■ ASSOCIATED CONTENT

Supporting Information

The Supporting Information is available free of charge at https://pubs.acs.org/doi/10.1021/acs.nanolett.0c04100.

> Comparison of colony size between *E. coli* cultured in LOW-MW resin vs BLEND-MW resin for 72 hours, comparison of surface areas for different construct geometries for ∼500 μL of the print volume, heat map and modeling for the COMSOL model of diffusion of a nutrient mimic, and Materials and Methods section (PDF)

■ AUTHOR INFORMATION

Corresponding Author

William F. Hynes − *Engineering Directorate, Lawrence Livermore National Laboratory, Livermore, California 94550, United States;* orcid.org/0000-0003-3628-9486; Email: hynes2@llnl.gov

Authors

Karen Dubbin − *Engineering Directorate, Lawrence Livermore National Laboratory, Livermore, California 94550, United States*

https://dx.doi.org/10.1021/acs.nanolett.0c04100
Nano Lett. 2021, 21, 1352−1359

Ziye Dong − *Physical and Life Sciences Directorate, Lawrence Livermore National Laboratory, Livermore, California 94550, United States;* orcid.org/0000-0002-0419-8523
Dan M. Park − *Physical and Life Sciences Directorate, Lawrence Livermore National Laboratory, Livermore, California 94550, United States;* orcid.org/0000-0002-6000-6805
Javier Alvarado − *Engineering Directorate, Lawrence Livermore National Laboratory, Livermore, California 94550, United States*
Jimmy Su − *Engineering Directorate, Lawrence Livermore National Laboratory, Livermore, California 94550, United States*
Elisa Wasson − *Engineering Directorate, Lawrence Livermore National Laboratory, Livermore, California 94550, United States*
Claire Robertson − *Engineering Directorate, Lawrence Livermore National Laboratory, Livermore, California 94550, United States*
Julie Jackson − *Engineering Directorate, Lawrence Livermore National Laboratory, Livermore, California 94550, United States*
Arpita Bose − *Department of Biology, Washington University, St. Louis, Missouri 63130, United States*
Monica L. Moya − *Engineering Directorate, Lawrence Livermore National Laboratory, Livermore, California 94550, United States*
Yongqin Jiao − *Physical and Life Sciences Directorate, Lawrence Livermore National Laboratory, Livermore, California 94550, United States;* orcid.org/0000-0002-6798-5823

Complete contact information is available at: https://pubs.acs.org/10.1021/acs.nanolett.0c04100

Author Contributions

The manuscript was written through contributions of all authors. All authors have given approval to the final version of the manuscript.

Notes

The authors declare no competing financial interest.

■ ACKNOWLEDGMENTS

This work was performed under the auspices of the U.S. Department of Energy by Lawrence Livermore National Laboratory under Contract DE-AC52-07NA27344. The research was supported by LLNL LDRD-20-ERD-013. IM#LLNL-JRNL-815557. The authors would like to thank Eric Duoss, Christopher Spadaccini, Maxim Shusteff, Shankar Sundaram, and Elizabeth Wheeler for their guidance and support in the conception of this project. We additionally would like to thank Wes Overton and Feliza Bourguet for their generosity in providing the *E. coli* strains used for printing, as well as Michael Guzman for assistance in preparing *E. coli* stocks.

■ ABBREVIATIONS

SLAM Bioprinting, Stereolithographic apparatus for microbial bioprinting; PμSL, Projection microstereolithography; PEGDa, Poly(ethylene glycol) diacrylate; SLA, Stereolithographic

■ REFERENCES

(1) Flemming, H. C.; Neu, T. R.; Wozniak, D. J. The EPS matrix: the "house of biofilm cells". *J. Bacteriol.* **2007**, *189* (22), 7945−7.
(2) Chandki, R.; Banthia, P.; Banthia, R. Biofilms: A microbial home. *J. Indian Soc. Periodontol* **2011**, *15* (2), 111−4.
(3) Wang, Z. W.; Chen, S. Potential of biofilm-based biofuel production. *Appl. Microbiol. Biotechnol.* **2009**, *83* (1), 1−18.
(4) Galie, S.; Garcia-Gutierrez, C.; Miguelez, E. M.; Villar, C. J.; Lombo, F. Biofilms in the Food Industry: Health Aspects and Control Methods. *Front. Microbiol.* **2018**, *9*, 898.
(5) Edwards, S. J.; Kjellerup, B. V. Applications of biofilms in bioremediation and biotransformation of persistent organic pollutants, pharmaceuticals/personal care products, and heavy metals. *Appl. Microbiol. Biotechnol.* **2013**, *97* (23), 9909−21.
(6) Kim, H. J.; Boedicker, J. Q.; Choi, J. W.; Ismagilov, R. F. Defined spatial structure stabilizes a synthetic multispecies bacterial community. *Proc. Natl. Acad. Sci. U. S. A.* **2008**, *105* (47), 18188−93.
(7) Flemming, H. C.; Wingender, J.; Szewzyk, U.; Steinberg, P.; Rice, S. A.; Kjelleberg, S. Biofilms: an emergent form of bacterial life. *Nat. Rev. Microbiol.* **2016**, *14* (9), 563−75.
(8) Fan, Y.; Xiao, Y.; Momeni, B.; Liu, Y. Y. Horizontal gene transfer can help maintain the equilibrium of microbial communities. *J. Theor. Biol.* **2018**, *454*, 53−59.
(9) Hoiby, N.; Bjarnsholt, T.; Givskov, M.; Molin, S.; Ciofu, O. Antibiotic resistance of bacterial biofilms. *Int. J. Antimicrob. Agents* **2010**, *35* (4), 322−32.
(10) Song, H.; Payne, S.; Gray, M.; You, L. Spatiotemporal modulation of biodiversity in a synthetic chemical-mediated ecosystem. *Nat. Chem. Biol.* **2009**, *5* (12), 929−35.
(11) Kassinger, S. J.; van Hoek, M. L. Biofilm architecture: An emerging synthetic biology target. *Synth Syst. Biotechnol* **2020**, *5* (1), 1−10.
(12) Nunan, N.; Wu, K.; Young, I. M.; Crawford, J. W.; Ritz, K. Spatial distribution of bacterial communities and their relationships with the micro-architecture of soil. *FEMS Microbiol. Ecol.* **2003**, *44* (2), 203−15.
(13) Lehner, B. A. E.; Schmieden, D. T.; Meyer, A. S. A Straightforward Approach for 3D Bacterial Printing. *ACS Synth. Biol.* **2017**, *6* (7), 1124−1130.
(14) Liu, X.; Yuk, H.; Lin, S.; Parada, G. A.; Tang, T. C.; Tham, E.; de la Fuente-Nunez, C.; Lu, T. K.; Zhao, X. 3D Printing of Living Responsive Materials and Devices. *Adv. Mater.* **2018**, *30* (4), 1704821.
(15) Saha, A.; Johnston, T. G.; Shafranek, R. T.; Goodman, C. J.; Zalatan, J. G.; Storti, D. W.; Ganter, M. A.; Nelson, A. Additive Manufacturing of Catalytically Active Living Materials. *ACS Appl. Mater. Interfaces* **2018**, *10* (16), 13373−13380.
(16) Qian, F.; Zhu, C.; Knipe, J. M.; Ruelas, S.; Stolaroff, J. K.; DeOtte, J. R.; Duoss, E. B.; Spadaccini, C. M.; Henard, C. A.; Guarnieri, M. T.; Baker, S. E. Direct Writing of Tunable Living Inks for Bioprocess Intensification. *Nano Lett.* **2019**, *19* (9), 5829−5835.
(17) Azeredo, J.; Azevedo, N. F.; Briandet, R.; Cerca, N.; Coenye, T.; Costa, A. R.; Desvaux, M.; Di Bonaventura, G.; Hebraud, M.; Jaglic, Z.; Kacaniova, M.; Knochel, S.; Lourenco, A.; Mergulhao, F.; Meyer, R. L.; Nychas, G.; Simões, M.; Tresse, O.; Sternberg, C. Critical review on biofilm methods. *Crit. Rev. Microbiol.* **2017**, *43* (3), 313−351.
(18) Kolesky, D. B.; Homan, K. A.; Skylar-Scott, M. A.; Lewis, J. A. Three-dimensional bioprinting of thick vascularized tissues. *Proc. Natl. Acad. Sci. U. S. A.* **2016**, *113* (12), 3179−84.
(19) Grigoryan, B.; Paulsen, S. J.; Corbett, D. C.; Sazer, D. W.; Fortin, C. L.; Zaita, A. J.; Greenfield, P. T.; Calafat, N. J.; Gounley, J. P.; Ta, A. H.; Johansson, F.; Randles, A.; Rosenkrantz, J. E.; Louis-Rosenberg, J. D.; Galie, P. A.; Stevens, K. R.; Miller, J. S. Multivascular networks and functional intravascular topologies within biocompatible hydrogels. *Science* **2019**, *364* (6439), 458−464.
(20) Laronda, M. M.; Rutz, A. L.; Xiao, S.; Whelan, K. A.; Duncan, F. E.; Roth, E. W.; Woodruff, T. K.; Shah, R. N. A bioprosthetic ovary

created using 3D printed microporous scaffolds restores ovarian function in sterilized mice. *Nat. Commun.* **2017**, *8*, 15261.
(21) Zhang, Y. S.; Yue, K.; Aleman, J.; Mollazadeh-Moghaddam, K.; Bakht, S. M.; Yang, J.; Jia, W.; Dell'Erba, V.; Assawes, P.; Shin, S. R.; Dokmeci, M. R.; Oklu, R.; Khademhosseini, A. 3D Bioprinting for Tissue and Organ Fabrication. *Ann. Biomed. Eng.* **2017**, *45* (1), 148−163.
(22) Raman, R.; Bashir, R. Stereolithographic 3D Bioprinting for Biomedical Applications. In *Essentials of 3D Biofabrication and Translation*; Atala, A., Yoo, J. J., Eds.; Academic Press: 2015; pp 89−121.
(23) Schaffner, M.; Ruhs, P. A.; Coulter, F.; Kilcher, S.; Studart, A. R. 3D printing of bacteria into functional complex materials. *Sci. Adv.* **2017**, *3* (12), No. eaao6804.
(24) Murga, R.; Stewart, P. S.; Daly, D. Quantitative analysis of biofilm thickness variability. *Biotechnol. Bioeng.* **1995**, *45* (6), 503−10.
(25) Mohammadi, Z.; Rabbani, M. Bacterial Bioprinting on a Flexible Substrate for Fabrication of a Colorimetric Temperature Indicator by Using a Commercial Inkjet Printer. *J. Med. Signals Sens* **2018**, *8* (3), 170−174.
(26) Cheptsov, V. S.; Churbanova, E. S.; Yusupov, V. I.; Gorlenko, M. V.; Lysak, L. V.; Minaev, N. V.; Bagratashvili, V. N.; Chichkov, B. N. Laser printing of microbial systems: effect of absorbing metal film. *Lett. Appl. Microbiol.* **2018**, *67* (6), 544−549.
(27) Cheptsov, V. S.; Tsypina, S. I.; Minaev, N. V.; Yusupov, V. I.; Chichkov, B. N. New microorganism isolation techniques with emphasis on laser printing. *Int. J. Bioprint* **2019**, *5* (1), 165.
(28) Hynes, W. F.; Chacón, J.; Segrè, D.; Marx, C. J.; Cady, N. C.; Harcombe, W. R. Bioprinting microbial communities to examine interspecies interactions in time and space. *Biomedical Physics & Engineering Express* **2018**, *4* (5), 055010.
(29) Xu, L.; Robert, L.; Ouyang, Q.; Taddei, F.; Chen, Y.; Lindner, A. B.; Baigl, D. Microcontact printing of living bacteria arrays with cellular resolution. *Nano Lett.* **2007**, *7* (7), 2068−2072.
(30) Connell, J. L.; Ritschdorff, E. T.; Whiteley, M.; Shear, J. B. 3D printing of microscopic bacterial communities. *Proc. Natl. Acad. Sci. U. S. A.* **2013**, *110* (46), 18380−5.
(31) Zheng, X.; Lee, H.; Weisgraber, T. H.; Shusteff, M.; DeOtte, J.; Duoss, E. B.; Kuntz, J. D.; Biener, M. M.; Ge, Q.; Jackson, J. A.; Kucheyev, S. O.; Fang, N. X.; Spadaccini, C. M. Ultralight, ultrastiff mechanical metamaterials. *Science* **2014**, *344* (6190), 1373−7.
(32) Zheng, X.; Smith, W.; Jackson, J.; Moran, B.; Cui, H.; Chen, D.; Ye, J.; Fang, N.; Rodriguez, N.; Weisgraber, T.; Spadaccini, C. M. Multiscale metallic metamaterials. *Nat. Mater.* **2016**, *15* (10), 1100−6.
(33) Jackson, J. A.; Messner, M. C.; Dudukovic, N. A.; Smith, W. L.; Bekker, L.; Moran, B.; Golobic, A. M.; Pascall, A. J.; Duoss, E. B.; Loh, K. J.; Spadaccini, C. M. Field responsive mechanical metamaterials. *Sci. Adv.* **2018**, *4* (12), No. eaau6419.
(34) Fairbanks, B. D.; Schwartz, M. P.; Bowman, C. N.; Anseth, K. S. Photoinitiated polymerization of PEG-diacrylate with lithium phenyl-2,4,6-trimethylbenzoylphosphinate: polymerization rate and cytocompatibility. *Biomaterials* **2009**, *30* (35), 6702−7.
(35) Brewer, A.; Dohnalkova, A.; Shutthanandan, V.; Kovarik, L.; Chang, E.; Sawvel, A. M.; Mason, H. E.; Reed, D.; Ye, C.; Hynes, W. F.; Lammers, L. N.; Park, D. M.; Jiao, Y. Microbe Encapsulation for Selective Rare-Earth Recovery from Electronic Waste Leachates. *Environ. Sci. Technol.* **2019**, *53* (23), 13888−13897.
(36) Samarasinghe, S. A.; Shao, Y.; Huang, P. J.; Pishko, M.; Chu, K. H.; Kameoka, J. Fabrication of Bacteria Environment Cubes with Dry Lift-Off Fabrication Process for Enhanced Nitrification. *PLoS One* **2016**, *11* (11), No. e0165839.
(37) Gordon, V. D.; Wang, L. Bacterial mechanosensing: the force will be with you, always. *J. Cell Sci.* **2019**, *132* (7), jcs227694.
(38) Lele, P. P.; Hosu, B. G.; Berg, H. C. Dynamics of mechanosensing in the bacterial flagellar motor. *Proc. Natl. Acad. Sci. U. S. A.* **2013**, *110* (29), 11839−44.
(39) Wickramasinghe, S. R.; Bower, S. E.; Chen, Z.; Mukherjee, A.; Husson, S. M. Relating the pore size distribution of ultrafiltration membranes to dextran rejection. *J. Membr. Sci.* **2009**, *340* (1−2), 1−8.
(40) Bush, B. G.; Shapiro, J. M.; DelRio, F. W.; Cook, R. F.; Oyen, M. L. Mechanical measurements of heterogeneity and length scale effects in PEG-based hydrogels. *Soft Matter* **2015**, *11* (36), 7191−200.
(41) Lin, S.; Sangaj, N.; Razafiarison, T.; Zhang, C.; Varghese, S. Influence of physical properties of biomaterials on cellular behavior. *Pharm. Res.* **2011**, *28* (6), 1422−30.
(42) Valentin, T. M.; DuBois, E. M.; Machnicki, C. E.; Bhaskar, D.; Cui, F. R.; Wong, I. Y. 3D printed self-adhesive PEGDA−PAA hydrogels as modular components for soft actuators and microfluidics. *Polym. Chem.* **2019**, *10*, 2015−2028.
(43) Belas, R. Biofilms, flagella, and mechanosensing of surfaces by bacteria. *Trends Microbiol.* **2014**, *22* (9), 517−27.
(44) Dufrene, Y. F.; Persat, A. Mechanomicrobiology: how bacteria sense and respond to forces. *Nat. Rev. Microbiol.* **2020**, *18* (4), 227−240.
(45) Wang, Y.; Guan, A.; Isayeva, I.; Vorvolakos, K.; Das, S.; Li, Z.; Phillips, K. S. Interactions of Staphylococcus aureus with ultrasoft hydrogel biomaterials. *Biomaterials* **2016**, *95*, 74−85.
(46) Ruhs, P. A.; Boni, L.; Fuller, G. G.; Inglis, R. F.; Fischer, P. In-situ quantification of the interfacial rheological response of bacterial biofilms to environmental stimuli. *PLoS One* **2013**, *8* (11), No. e78524.
(47) Pavlovsky, L.; Younger, J. G.; Solomon, M. J. In situ rheology of Staphylococcus epidermidis bacterial biofilms. *Soft Matter* **2013**, *9* (1), 122−131.
(48) Tuson, H. H.; Auer, G. K.; Renner, L. D.; Hasebe, M.; Tropini, C.; Salick, M.; Crone, W. C.; Gopinathan, A.; Huang, K. C.; Weibel, D. B. Measuring the stiffness of bacterial cells from growth rates in hydrogels of tunable elasticity. *Mol. Microbiol.* **2012**, *84* (5), 874−91.
(49) Haque, N.; Hughes, A.; Lim, S.; Vernon, C. Rare Earth Elements: Overview of Mining, Mineralogy, Uses, Sustainability and Environmental Impact. *Resources* **2014**, *3* (4), 614−635.
(50) Liu, C.; Yan, Q.; Zhang, X.; Lei, L.; Xiao, C. Efficient Recovery of End-of-Life NdFeB Permanent Magnets by Selective Leaching with Deep Eutectic Solvents. *Environ. Sci. Technol.* **2020**, *54* (16), 10370−10379.
(51) Zhou, B.; Li, Z.; Chen, C. Global Potential of Rare Earth Resources and Rare Earth Demand from Clean Technologies. *Minerals* **2017**, *7* (11), 203.
(52) Dinocourt, C.; Legrand, M.; Dublineau, I.; Lestaevel, P. The neurotoxicology of uranium. *Toxicology* **2015**, *337*, 58−71.
(53) Park, D. M.; Taffet, M. J. Combinatorial Sensor Design in Caulobacter crescentus for Selective Environmental Uranium Detection. *ACS Synth. Biol.* **2019**, *8* (4), 807−817.

https://dx.doi.org/10.1021/acs.nanolett.0c04100
Nano Lett. 2021, 21, 1352−1359